Damage Characterisation and Mechanical Behaviour of Ultra-Thick Composite Laminates Subjected to Low-Velocity In-Plane Impact

Mitchell J. van Donselaar[1]

The University of New South Wales at the Australian Defence Force Academy

The manufacture of traditional marine propellers has long consisted of alloys including Nickel-Aluminium-Bronze or Manganese-Aluminium-Bronze which have inherent limitations including fixed shape, undesirable magnetic properties, and corrosion susceptibility. Advanced fibre-reinforced composite materials have favourable properties including high strength-to-weight ratios, corrosion resistance, and magnetic properties and are being investigated to challenge traditional propeller manufacture. However, susceptibility to impact events is one issue that is not well understood for composite marine propellers. The aim of this study is to examine and characterise the damage and mechanical behaviour of ultra-thick composite laminates which are used for marine propellers, when subjected to low-velocity in-plane impact. The use of an analytical background, experimental drop-weight testing and numerical simulations formed the structure for the study. The study found that the use of modified Hertzian contact laws by Tan and Sun for a hemispherical impactor and Nelson Norden for a cylindrical impactor were accurate until the damage limit threshold in testing. Using the high-speed footage and post-impact specimen observations the damage for impact events was characterised. This involved the escalating progression of local stress whitening, local delaminations, propagation of delaminations with fibre and matrix crushing in the local impact area. Numerical results determined that the composite was far more damage resistant to impact across-plies than along plies when subjected to cross-thickness impact. These results from this study are useful in understanding the damage mechanisms and mechanical response of ultra-thick composite laminates subjected to in-plane impact, however, additional study is recommended before conclusions are made for the direct application to marine propellers.

Contents

[1] SBLT, School of Engineering & Information Technology. ZEIT4501

Nomenclature

E	=	Modulus of Elasticity (GPa)
E_r	=	stiffness of impactor material (MPa)
E_p	=	stiffness of target material (MPa)
F	=	applied contact (indentation) force (N)
R	=	indenter radius (mm)
L	=	length of contact area (mm)
v_r	=	Poisson's ratio of impactor
v_p	=	Poisson's ratio of target
G	=	in-plane shear modulus (GPa)
δ	=	indentation depth (mm)
X^T	=	longitudinal tensile strength (MPa)
X^C	=	longitudinal compressive strength (MPa)
Y^T	=	transverse tensile strength (MPa)
Y^C	=	transverse compressive strength (MPa)
S^L	=	longitudinal shear strength (MPa)
S^T	=	transverse shear strength (MPa)
α	=	coefficient that determines the contribution of shear stress to the fibre tensile initiation criterion
$\hat{\sigma}_{11}, \hat{\sigma}_{22}, \hat{\tau}_{12}$	=	components of the effective stress tensor, $\hat{\sigma}$, that is used to evaluate the initiation criteria
σ	=	true stress
M	=	damage operator
d_f	=	internal fibre damage variable
d_m	=	internal matrix damage variable
d_s	=	internal shear damage variable
11	=	principal material direction 1
22	=	principal material direction 2
33	=	principal material direction 3
12	=	principal plane 12
13	=	principal plane 13
CTI	=	Cross-thickness impactor
x^t	=	tension
x^c	=	compression

I. Introduction

Composite materials have been increasingly applied in the maritime industry due to the need for vessels that are of lighter weight, increased operational performance and lower overall lifecycle costs. They are already ubiquitous with pleasure boat and racing yacht construction and widely used in construction of fast ferries, naval and coastguard patrol craft, fishing and work boats and offshore oil and gas industry. Marine propellers are one additional marine structure where use of composite materials is favourable. There are several advantages which fibre-reinforced composites inherently provide over alloys which are conventionally used for marine propellers. These include flexibility, low weight, corrosion resistance, ageing resistance, large number of materials and layup combinations to choose from, ability to optimise design to cater to many different design goals and ease to achieve smoother surface finishes with high manufacturing tolerances. These characteristics transfer directly to marine propeller applications giving the particular advantages of shape adaptability, weight and inertia reduction, corrosion resistance, enhanced stealth capabilities due to composites typically being non-magnetic, low sound generation and turbulence due to flexibility, a large choice of materials and layup conditions that can be optimised for performance and a lower risk of cavitation [1-3]. Typically, composite marine propellers that have been manufactured previously have been primarily for reasons other than their potential for shape adaptability. In 2003, QinetiQ completed sea trials for a 2.9 diameter composite propeller with their 90m long trimaran warship prototype the RV Triton. During the trial, they realised some benefits including the light weight of composite material allowing blades to be thicker in order to reduce cavitation, improved strength compared to the previous NAB propeller, and improved life expectancy of composite propellers. There has also been other significant investigations into composite propellers by several navies including those from Germany, the United Kingdom, the United States of America, and the Netherlands [4, 5]. The dynamic nature of the maritime environment necessitates that these marine composites be able to withstand high magnitude dynamic loading conditions. Consequently, they are typically large and relatively thick where the effect of thickness can no longer be ignored. In the aerospace industry where composites are often utilised in thin panels there has been little need for study of thickness effects [6]. The lack of information results in large safety factors being used when composites are proposed for marine applications. These often range from 4-6 with static loads and up to 10 for dynamic loads [1]. Importantly, end users of marine composites are interested in the characterisation of interlaminar behaviour for several reasons: First, to be able to supply input data for design and optimisation calculations and hence reduce the risk of delamination in service. Second, to be able to characterise a new material and compare its behaviour to that of existing materials - these properties are strongly related to fibre/ matrix interface quality which is very difficult to measure directly. Third, to check fabrication quality as interlaminar fracture behaviour is very sensitive to defects [1].

II. Analytical

Impact occurrences are a regular phenomenon which occur in many industries; however, their presence is generally undesirable due to impact phenomena and the induced damage that can occur during an impact event. The importance of characteristic material behaviour of the target and impactor was outlined by Backman and Goldsmith [7], and the material response in different impact events were classified. These include firstly the elastic response of projectile and target, secondly the plastic deformation in the target, and thirdly the target penetration or propagation in elastic and plastic conditions. In impact cases, there are two important factors that must be considered: the contact behaviour and the damage mechanisms of the materials involved. For the case in this study, the impactor is assumed to be rigid with no requirement to consider its damage mechanisms.

Low-velocity impact responses of targets have also been assumed to behave similarly to quasi-static load responses in many impact events. It has also been proposed that low-velocity drop weight and quasi-static tests be used to examine the similarity and distinct behaviours by several researchers [8-13]. Quasi-static testing is used in literature for several reasons when relating to impact studies. First, it is easier to develop a preliminary understanding of damage mechanisms and characteristics by executing a quasi-static test in a controlled manner. Secondly, quasi-static tests can be treated as very low velocity impacts when examining the effect of impact velocity on damage. Thirdly, it makes examination of the onset of damage possible without the use of a high-speed camera. Finally, it is a method to measure contact stiffness which is required for theoretical analysis and FEM [11]. It has also been shown that quasi static indentation can be used to find the contact behaviour of composite laminates subjected to low velocity impact. In particular, the damage threshold limit can be determined from the curve of indentation force-displacement of the indenter. In a study by Shen et al, the damage threshold limit for a 4mm laminate subjected to low velocity impact was determined within 10% by using quasi static indentation at a rate of 12mm/min. The 10% difference was considered acceptable due to the complexity in determining the delamination threshold load [14]. The damage threshold limit is one characteristic that can be useful in assessing the resistance of a composite laminate to such events. The damage threshold limit is defined as the first sudden load drop in the impact force history that is associated with delamination and is well

documented in literature [15-17]. An increased damage threshold limit indicates an increased damage resistance property and is favourable for the avoidance of damage during an impact event.

The contact behaviour during an impact is an important aspect, since its nature affects the damage mechanisms involved and is largely a function of the impactors geometry, density and hardness [15]. The first satisfactory elastic contact model was developed by Hertz, and was derived assuming contact between two smooth elastic, homogenous, isotropic solid bodies of revolution [18, 19]. This model has been modified numerous times for varying geometries and materials [20-23]. However, there are two versions that are considered in this study. Tan and Sun proposed a modification based on the experimental static loadings of composite laminates. The model considers a hemispherical indenter contacting an infinite-width flat composite plate. The equations for the model are listed below and will be used for results analysis in this study:

$$F = k\delta^n \qquad k = \frac{\frac{4}{3}\left(R^{\frac{1}{2}}\right)}{\frac{1-v_i^2}{E_r}+\frac{1}{E_p}} \tag{1}$$

This model has been modified by others to consider laminates of finite thickness rather than a semi-infinite elastic body. However, it was found that when the indenter is small relative to the plate thickness, the relative effect of the correction is minimal [24]. An experimental study by Sutherland and Soares [18] found that the indentation law fit well at small loads; however, they observed that at large loads where intensive damage occurred there was a significant deviation observed. A similar study by Wu and Shyu [25] reported that the power law for the force-indentation relationship was not applicable after fibre-splitting and delamination occurred in laminates.

Prof Lee and Prof Liu [26] compared the indentation of cross-ply glass/epoxy laminates subjected to static loading with a 6.35mm hemispherical tip in both out-of-plane and edge loading. They found that the edge indentation was smaller than the out-of-plane indentation when subjected to the same peak force. They attributed the higher resistance to static indentation to the loading direction of the fibres in the laminate and the larger Young's modulus of the specimen in the lamina plane. The result from the static edge indentation tests also demonstrated a different indentation law for those from out-of-plane indentation tests. They also noted that the different local damages required further study to understand the deviation between out-of-plane and edge indentation. Malhotra and Guild also studied the effect of impact location between central, near edge and on-edge impact, they found that the results for central and near-edge impact were very similar. However, a higher maximum force and differing damage mechanisms including damaged fibres were recorded for the on-edge tests due to the increased elastic modulus in-plane [27]. Cai et al studied the damage behaviour of laminated e-glass epoxy beams with an initial delamination subjected to an axial impact both experimentally and numerically. They noted that delaminations and matrix cracking where the dominant behaviour of the beams under axial impact. The propagation of the initial delamination was the main damage behaviour which decreased the load carrying capacity of the beams [28].

The Hertzian contact law was also modified by Nelson Norden [23] for the contact between a cylinder and plane surface of finite length. The equations for this derivation are listed below and will also be used for results analysis in this study:

$$\delta = \frac{F}{L}(\lambda_r + \lambda_p)\left(1 + \ln\left(\frac{L^3}{(\lambda_r+\lambda_p)FR}\right)\right) \qquad \lambda_i = \frac{1-v_i^2}{\pi E} \tag{2}$$

The case for 'impact of marine composites' includes a great variety of possible impactors. Waterways contain a large range of objects that have the potential to damage marine composites, and include a wide range of impactor hardness, density and shapes [3]. For this study, two impactors are chosen: a 20mm hemispherical impactor and a 20mm diameter cylinder, herein referred to as the cross-thickness impactor (CTI). The hemispherical impactor was chosen due to it being readily available in the impactor dynamics laboratory at UNSW Canberra. In their study, Goldsmith included hemispherical impactors in the category of most common geometric shapes for projectile noses, and hemispherical impactors are widely used in impact testing [8, 10, 12, 15, 18, 24, 26, 29, 30]. The use of the 20mm diameter hemispherical impactor in this study provides a generic geometric shape which can be easily understood with Hertzian contact laws and later used as the basis for study of other impactor shapes. The cross-thickness impactor is used to simulate impact across the width of the composite. This is both relevant for the case of a leading edge of a propeller being struck and also enables study for the effect of line-of-impact relative to the lamina stacking direction. The cross-thickness impactor also provides the means to study the impact scenario where the impact location is not localised in the centre of the target and protrudes to the edge of the target. This is the likely case in a propeller strike where the leading or trailing edge of the propeller, under forward or reverse operation respectively, strikes a piece of underwater debris.

There are several energy absorption mechanisms in fibre composites when subjected to low velocity impact. These include matrix fracture, fibre deformation and breakage, friction, fibre/matrix debonding and delamination. [31] Delamination is caused by high interlaminar stresses as well as low through-thickness debonding resistance. Interlaminar stresses develop when there is a sizeable difference in the elastic properties of two successive lamina. Usually this strength discrepancy comes from a large change in the fibre directions across two neighbouring lamina. The interlaminar strength of laminates if a function of many factors, and thus it is important to be able to accurately characterise and define it. Baley [1] discussed a number of tests useful for characterising the interlaminar behaviour. Matrix cracking and fibre breakage typically occur on laminate surfaces either where bending stresses are at a maximum or where there is a high local contact stress. These are easily identified by a visual inspection as it manifests itself in a stress-whitened or discoloured patch. In early work it was demonstrated that delamination is a crucial limiting factor for composites subjected to low velocity impact. The interlaminar strength of laminates which resists delaminations is a function of the components (matrix, fibres, fibre-matrix interface), type of reinforcement (mat, woven, combination), stacking sequence, fabrication quality, ageing (exposure to the maritime environment) and type of loading [32-34]. Studies have also described methods to improve delamination resistance including: tougher matrix polymers, tough interleaf layers, through-thickness reinforcements (stitching, inserts, pins, 3D stitching), improved fibre/ matrix strength (fibre surface modification, interphase creation) and optimisation of fabrication [35-39].

The defining property which makes a composite 'thick', is that the effects of its thickness can no longer be ignored. The increased thickness of marine composites leads to a range of complications particularly in manufacturing and mechanical properties. Difficulties in manufacture can lead to a range of defects. The residual stress caused by differing cure kinetics across the laminate thickness can lead to micro-cracks, delaminations, fibre waviness and warpage. The greater thickness due to an increased number of plies also makes consolidation more difficult increasing the risk of voids, regions with low fibre fractions, fibre waviness and resin rich zones. All of these undesirable effects can reduce the important properties of the laminate [6, 40-43].

The damage mechanisms for the composite laminate in this study is considered using the failure criteria developed by Hashin [44]. The failure criteria were established in terms of quadratic stress polynomials which were expressed in transversely isotropic invariants of the applied stress state. In the theory, there are four distinct and separate failure modes for tensile and compressive fibre and matrix modes resulting in a piecewise smooth failure surface. The damage criteria have the following forms [44, 45]:

Failure Mode	**Equation**	
Fiber tension $(\hat{\sigma}_{11} \geq 0)$	$F_f^t = \left(\frac{\hat{\sigma}_{11}}{X^T}\right)^2 + \alpha\left(\frac{\hat{\tau}_{12}}{S^L}\right)^2$	(3)
Fiber compression $(\hat{\sigma}_{11} < 0)$	$F_f^c = \left(\frac{\hat{\sigma}_{11}}{X^C}\right)^2$	(4)
Matrix tension $(\hat{\sigma}_{22} \geq 0)$	$F_m^t = \left(\frac{\hat{\sigma}_{22}}{Y^T}\right)^2 + \left(\frac{\hat{\tau}_{12}}{S^L}\right)^2$	(5)
Matrix compression $(\hat{\sigma}_{22} < 0)$	$F_m^c = \left(\frac{\hat{\sigma}_{22}}{2S^T}\right)^2 + \frac{\left[\left(\frac{Y^C}{2S^T}\right)^2 - 1\right]\hat{\sigma}_{22}}{Y^c} + \left(\frac{\hat{\tau}_{12}}{S^L}\right)^2$	(6)
	Where $\hat{\sigma} = M\sigma$	(7)
$M = \begin{bmatrix} \frac{1}{1-d_f} & 0 & 0 \\ 0 & \frac{1}{1-d_m} & 0 \\ 0 & 0 & \frac{1}{1-d_s} \end{bmatrix}$	$d_f = \begin{cases} d_f^t \; if \; \sigma_{11} \geq 0 \\ d_f^c \; if \; \sigma_{11} < 0 \end{cases}$ $d_m = \begin{cases} d_m^t \; if \; \sigma_{22} \geq 0 \\ d_m^c \; if \; \sigma_{22} < 0 \end{cases}$ $d_s = 1 - (1 - d_f^t)(1 - d_f^c)(1 - d_m^t)(1 - d_m^c)$	(8)

How the material is affected after damage initiation occurs is determined by damage evolution criteria. In Abaqus, the damage evolution is tracked by the calculation of equivalent stresses and strains in an element. While the determination of the onset of damage is stress based, the damage growth model is strain based. The model assumes that damage is characterised by progressive degradation of material stiffness which leads to material failure [46, 47].

III. Experimental

A. Method and Materials

1. Specimen Preparation

The composite material was fabricated using vacuum resin infusion method with an initial target thickness of 40mm. After infusion, the sample was cured at room temperature overnight, then post cured at $50°C$ for 5 hours. The surfaces of the panel were then levelled flat using a 3-axis CNC router. The remaining fabric was then laid up to achieve a final thickness of 75-80mm, infused with resin, then cured again at room temperature overnight. Finally, the panel was post-cured at $50°C$ for 12 hours. The post-cure at $50°C$ after cure at ambient temperature is recommended by the resin manufacturer to obtain optimum mechanical and distortion properties along with lessening of brittle behaviour [48]. A waterjet cutter was then used to trim the panel and obtain strips which were cut square by the CNC router. Individual samples were then cut from the strips using a water-cooled diamond saw. The final sample sizes were cut to cubes with side lengths of 50mm at varying lamina angles of $0°, 22.5°, 45°$ and $67.5°$. Photos taken during manufacture can be found in Figure 1.

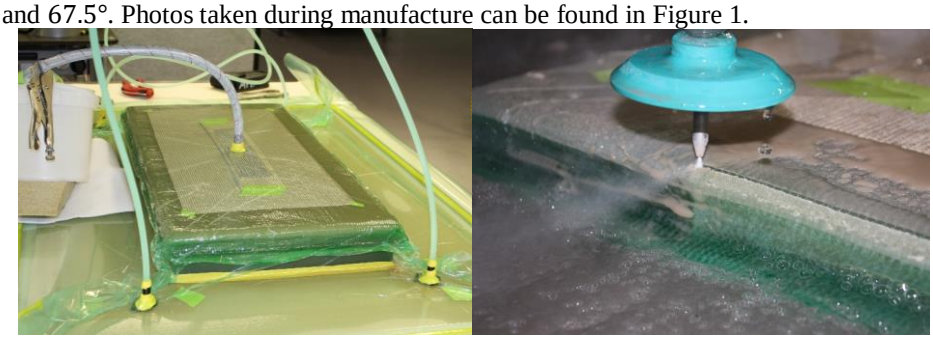

Figure 1. Photo of the composite block during infusion in the second stage (left), photo of the composite block being cut to size by the waterjet cutter (right)

2. Materials

The fabric used for manufacture of the samples was Stitched Quadriaxial $(0°, 90°, \pm 45°)$ E-glass $1205\ g/m^2$ manufactured by Colan Australia [49]. The resin used was the Kinetix R118 infusion resin which was paired with the H103 hardener, both manufactured by ATL Composites. The Kinetix R118 infusion system has received a Lloyd's Register Certificate of Approval for the Rules and Regulations for Classification of Special Service Craft and is appropriate for marine use [50, 51] thus it is appropriate for marine applications. The properties for this material are detailed in Table 1 and Table 2.

Figure 2. Image of the Instron CEAST 9350 drop tower

3. Method

For the experimental testing the an Instron CEAST 9350 Drop Tower Impact System in the Impact Dynamics laboratory at UNSW Canberra was used. An image of the drop tower is shown in Figure 2, and a diagram showing how the impactor strikes the sample is shown in Figure 3. 500kHz sampling for the impact force-data and high-speed footage of the impact events was captured and used for later analysis. There were 19 experimental tests performed, all with the 20mm hemispherical impactor. The 0° samples were tested at 5, 6.25, 7.5 and 8.75m/s while the other angled samples were tested at 5, 6.25 and 7.5m/s.

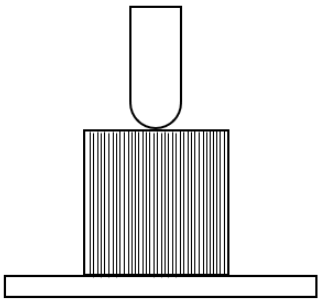

Figure 3. Diagram of impact set-up with impactor (top) impacting the 0° sample (middle) in-plane on the base (bottom)

B. Results

4. 0° Sample Results

From Figure 4, it can be seen that there is an escalating level of visible damage present as the impact velocity increases. At 5m/s there is a small patch of stress-whitening at the area of impact, with some delaminations observable only with the use of backlighting. At 6.25m/s the size intensity of the stress whitening at the impact site increased with delaminations that extend the full width of the sample visible without the use of backlighting. At 7.5m/s the stress-whitened area includes areas with small amounts of fibre and matrix crushing present. At one test at 7.5m/s the sample remained intact as one piece but for the other test it separated. At 8.75m/s there is significant fibre and matrix crushing present at the impact site along with the stress whitening and the samples split in both of the tests.

The high-speed footage did not show any damage for the 5m/s tests but was useful in identifying damage in the others. For the 6.25m/s test, the larger delamination seen in the backlit figure is visible but difficult to see in the footage. The high-speed footage for 7.5m/s test 2 shown in Figure 5 revealed an interesting phenomenon that would have remained unknown otherwise. During the impact, a delamination initiates in the location shown by the red arrow in frame 0.9ms. The sample then begins to split along that delamination to a maximum separation of 3.65mm as shown in frame 1.9ms. During the separation, there are fibres that are connected to both the left and right side of the sample being separated. These fibres oppose the separation of the sample and once the sample reaches the maximum separation of 3.65mm it begins to close due to the action of the fibres. The separation at 1.9ms and 3.6ms are shown by the red arrows in both frames. The footage for 8.75m/s test 1 shown in Figure 6 shows the damage behaviour for a complete failure. In frame 0.5ms, the delaminations can be seen as they start to grow to the width and depth of the sample. At 1ms the delamination has fully developed, and the sample has started to split into two pieces with only fibres connecting the pair. In frame 1.5ms the sample has continued to separate and the 'tearing motion' that held the sample together in 7.5m/s test 2 can be seen clearly. From the damage observation using backlighting and the high-speed footage it is interesting to note the location of delaminations relative to the location of impact. The delaminations do not occur in the centre of the impact site, but rather between 3-5mm away from the centre. This is due to fibre buckling occurring under the impactor where indentation occurs which causes the delamination to be located offset from the centre of the impactor. This phenomenon is discussed later during numerical simulations.

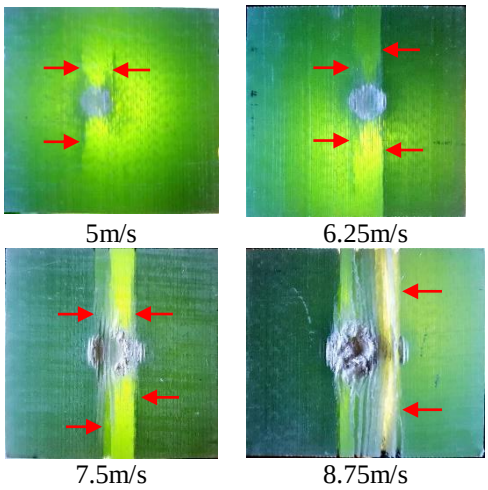

Figure 4. Photos of samples from 0° experimental testing using single-source backlighting to highlight delaminations

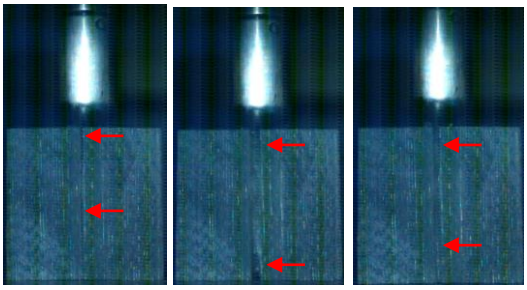

Figure 5. High-speed footage from 7.5m/s test 2

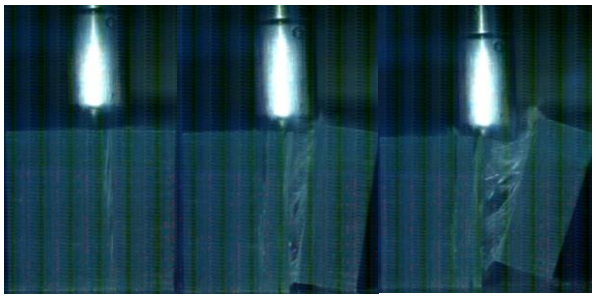

Figure 6. High speed footage from 8.75m/s test 1

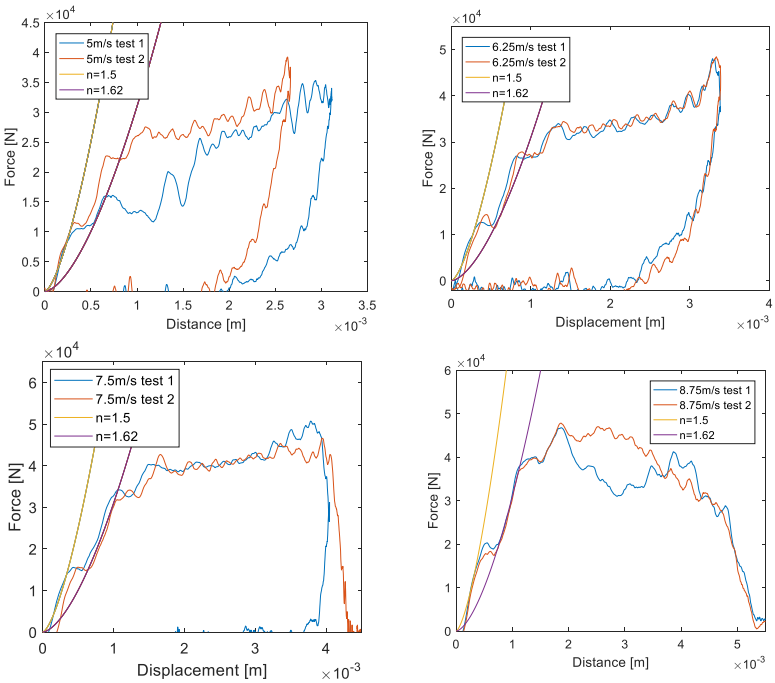

Figure 7. Force-displacement plots for hemispherical impact of 0° samples

When comparing the force-displacement plots for experimental tests to the Hertzian contact law modified by Tan and Sun [46] it can be seen in Figure 7 that the value for n=1.5 matches the slope well before the first inconsistency in the plot. The value for n=1.62 then fits the curve well until the second

inconsistency where the plot starts to flatten out and is not well matched by the modified contact law with any *n* value. The existence of the first inconsistency in the force plot is not consistent with other studies for both low-velocity impact and quasi-static indentation or the numerical results presented. It is suspected that this is due to the experimental setup used and that the second inconsistency where the force-displacement plot changes direction significantly is the actual damage threshold limit. The similarity between the force-displacement data and contact law in these results are consistent with results from previous studies which suggested that the indentation law fits well at small loads, but not at larger loads where fibre-splitting, delamination and intensive damage occurs [18, 25].

5. Mixed angle samples results

For the mixed angled testing, 22.5° samples exhibited delaminations in all tests, and separated into two at 6.25 and 7.5m/s. The 45° samples did not show any visible delaminations at 5m/s, but at 6.25m/s there were notable delaminations, with one of the samples separating, and at 7.5m/s both samples separated. The 67.5° samples did not exhibit any damage except local stress whitening at the impact site at 5 or 6.25m/s. The damage progression was similar to the 0° samples which escalated in order of local stress whitening at the impact site, small delaminations near impact site, propagation of delaminations across depth and width of samples then fibre and matrix crushing at the impact site where high contact stresses were present. The high-speed footage for the mixed angled samples supports this with the propagation of delaminations observable. For the 6.25m/s test of the 22.5°

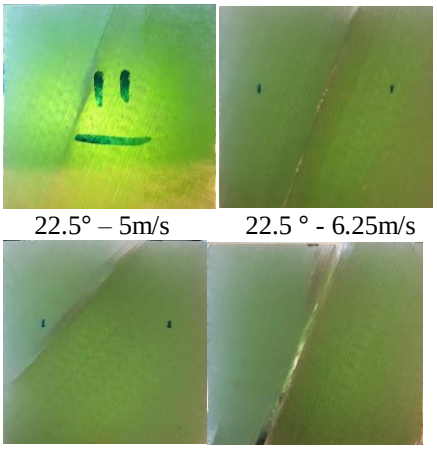

Figure 5. Photos of samples from mixed angle experimental testing using single-source backlighting to highlight delaminations

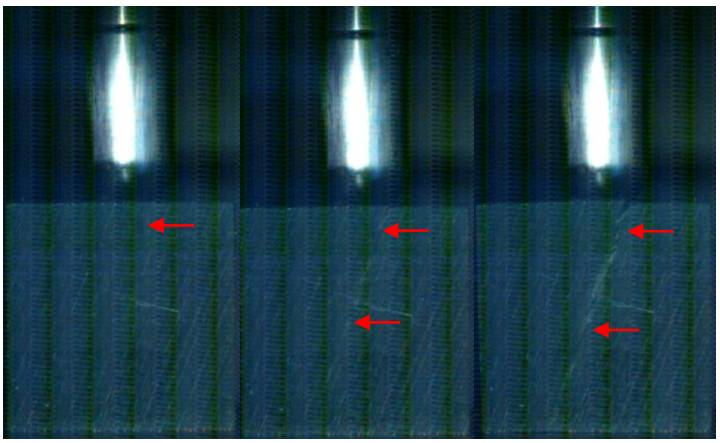

Figure 6. High-speed footage for the 22.5° sample at 6.25m/s

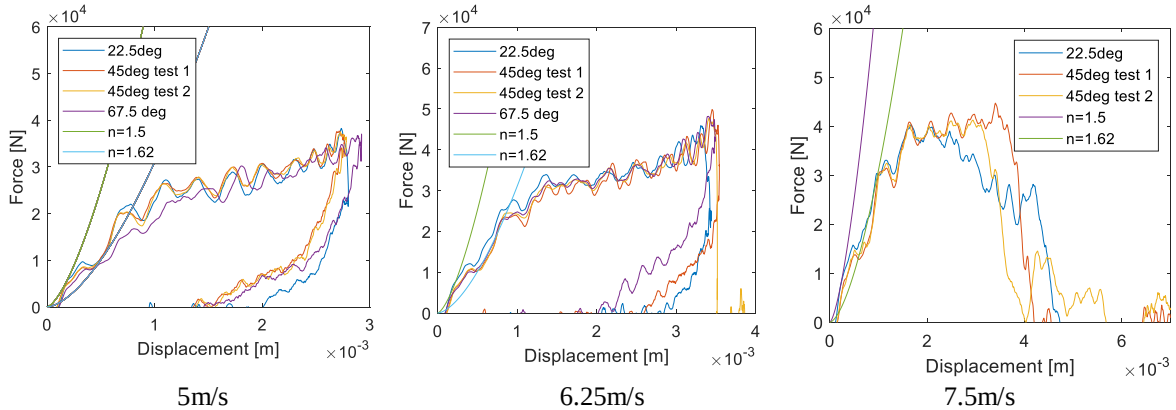

Figure 7. Force-displacement plots for mixed angled tests with hemispherical impactor

sample shown in Figure 6, there is a noticeable change in colour through the sample at 0.8ms indicating the conception of a delamination. In the next frame at 0.9ms the delamination has propagated to the face closest to the camera and by 1.2ms the delamination has propagated the whole depth of the sample. As seen in Figure 7

the force-displacement plots are very similar for each angle tested and suggest the gross mechanical response and damage threshold limits are similar for any impact angle. However, the damage behaviour once the samples passed the threshold is most evident in 22.5° samples followed by 45° and 67.5° samples. It was also evident from the samples post-impact that there was a change in primary damage behaviour for the 45° samples. For the samples that failed at 45° the high-speed footage revealed an increase in the effect of shear force. When the samples failed they followed the direction of the impactor and the corner sheared from the main body of the sample as shown Figure 8. This reinforces the importance of a complete interlaminar definition including both interlaminar shear and normal strengths when defining material properties and considering in-plane impact.

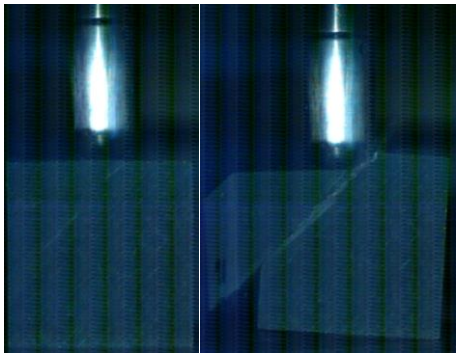

0.5ms 1.3ms

Figure 8. High-speed footage of 45° sample at 7.5m/s

IV. Numerical Model

A. Model Formulation

In this study, the software Abaqus/Explicit was used to model and analyse the ultra-thick composite subjected to low-velocity in-plane impact. Using the embedded graphical user interface and Catia v5, the 3D model was generated. Following an early investigation, a mixed-modelling, or meso-scale, technique was chosen where each lamina was modelled as a discrete, macroscopically modelled layer.

Models for each lamina angle of $0°, 22.5°, 45°$ and $67.5°$ were generated with each lamina being 1.1mm thick to simulate the experimental samples as shown in Figure 9. The impactors and base were modelled as rigid elements, since previous studies had found minimal difference between the use of a steel and rigid impactor, and the use of a rigid impactor would reduce the computational time [24, 30]. The impactors used in numerical simulations were a 20mm hemispherical impactor to replicate experimental results and a 20mm cylinder, also referred to as a cross-thickness impactor. The material properties for the lamina were defined using the Hashin damage model, and values are outlined in Table 1 and the lamina were modelled using SC8R elements which are 8-node quadrilateral in-plane general purpose continuum shell elements. The properties for the definition of lamina-to-lamina and lamina-to-impactor/base interactions are included in Table 2. The material properties were provided by Dr Nigel St John and Dr Andrew Phillips [52] and were compared to values found in literature to verify [53, 54]. No material property testing of the samples was conducted in this study, however, to improve the numerical model it is recommended to test the experimental samples for interlaminar shear and normal strength using tests suggested by Baley et al [1].

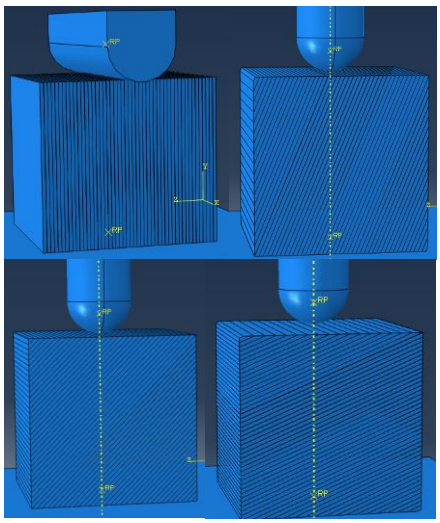

Figure 9. Screenshots of assembly for four different model angles

Table 1. Values used to define properties of lamina in the numerical model

Hashin Damage	
Property	**Value**
Longitudinal Strength	277 MPa
Transverse Strength	252 MPa
Longitudinal Shear Strength	100 MPa
Transverse Shear Strength	53 MPa
Density	
Density	1850 kg/m^3
Elastic	
Type	Lamina
E_{11}	14.6 MPa
E_{22}	14.3 MPa
v_{12}	0.18
G_{12}	6.1GPa
G_{13} & G_{23}	4.5GPa

Due to limitations for the number of nodes in the version of Abaqus available the element size for the lamina was limited to 1.65mm. This mesh was satisfactory, however post-processing with Savitzky-Golay smoothing was used to remove excessive noise from the data. Simulations using a finer mesh with element size of 1mm were conducted through another licence in Abaqus and provided more accurate results more similar to the experimental values. The difference between the best mesh tested and experimental results can be attributed to uncertainty in material properties and that the base support in experimental testing was not perfectly rigid. While the mesh used was not as accurate as using the finer mesh, the trends identified in numerical simulations that duplicated the experimental tests were similar and were thus

satisfactory for the identification of trends in other tests. The comparison between the mesh used and experimental result is shown in Figure 10 while a comparison between the best mesh tested and the experimental results is shown in Figure 12.

Table 2. Values used to determine properties for lamina-to-lamina and lamina-to-impactor/base in the model

Lamina-to-lamina	
Property	**Value**
Damage Initiation Criterion	Quadratic traction
Normal Damage	100 MPa
Shear Damage	100 MPa
Specify mixed mode behaviour	Benzeggagh-Kenane
Power-law/BK constant	1.45
Lamina-to-impactor/base	
Friction formulation	Penalty
Directionality	Isotropic

B. Results

For the numerical results for hemispherical impact of the 0° samples the development of elastic impact at 1.25m/s to sample failure at 8.75m/s is clear in the force-displacement data in Figure 12. The 1.25m/s plot is barely distinguishable because the loading and unloading of the impactor follow the same path in the force-displacement plot. The 2.5m/s result shows some deviation between the loading and unloading, and this continues until the 5m/s which exhibited significant difference between unloading and loading. The 6.25m/s test shows the impactor returning however this was only after the sample had split due to delaminations. In the 7.5m/s and 8.75m/s tests the impactor does not rebound as the sample split due to intense delaminations and separation. All the 0° tests exhibit a similar damage threshold limit at 34kN except the 3.75m/s sample which exhibited a damage threshold limit of 40kN due to excessive noise in the original data. All the tests follow the Tan and Sun indentation law with n=1.62 until the damage threshold limit as per experimental results.

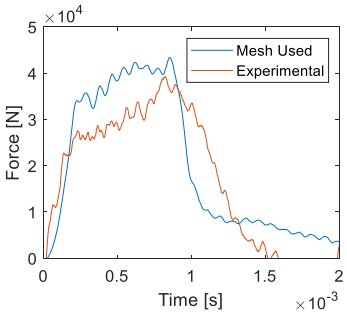

Figure 10. Comparison of mesh used and experimental results

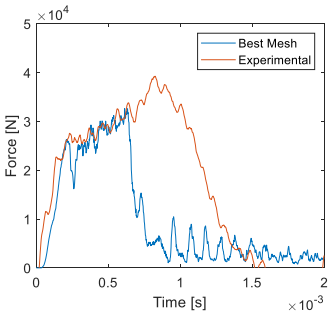

Figure 11. Comparison of best mesh tested and experimental results

The cross-thickness impact of the 0° samples compared the effect of impactor orientation relative to the lamina stacking direction. As shown in Figure 14, when the CTI impacted the sample along the plies at 0° relative to the lamina the samples exhibited significantly more damage than when impacted across the plies at 90°. Impact of the CTI at 45° exhibited similar behaviour to the 90° tests, however at 7.5m/s the unloading force occurs without change in displacement due to significant damage caused in the test. It is important to note since the samples were modelled as 50mm cubes that the contact length for the 0° and 90° tests was 50mm but the 45° test had a contact length of 70.7mm due to contact along the diagonal. Since delamination was shown to be the dominant damage mechanism in both experimental and numerical hemispherical testing, it was expected that the CTI impact at 0° would encourage this same failure since the contact stresses were concentrated along the plies. The impacts of the CTI at 45° and 90° only provided a small contact stress at each interlaminar interface and consequently there was

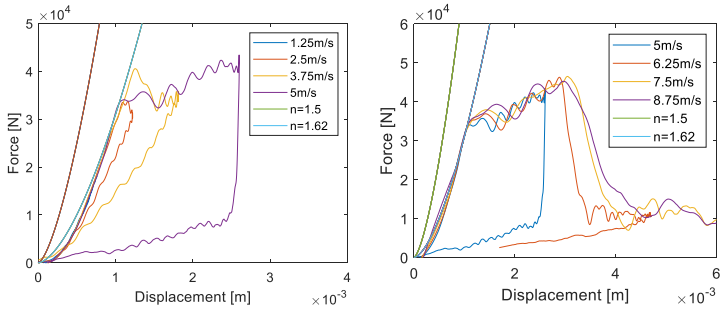

Figure 12. Force-displacement plots for hemispherical impact of 0° samples

significantly less damage and a much higher delamination threshold limit of >250kN compared to 115kN for the 0° impact. In all CTI tests of 0° samples however, it is important to note that they all followed the contact law for cylinder-plane impact derived by Nelson Norden despite having different damage threshold limits. The CTI impact of mixed angled samples provided the same conclusions as the 0° samples. The interlaminar interface was the limiting factor, and due to the to the geometry of the samples modelled, each sample orientation had a varying interlaminar contact area following experimental sample geometry. In the mixed angle tests the 0° and 22.5° samples fit the indentation law well until 50kN for along ply tests, while for across ply tests the 0° sample followed the indentation law until 190kN and the 22.5° sample followed it until its damage threshold limit at 115kN. The higher angled samples did not follow the indentation law well. This is due to the elastic modulus used for calculation being for the in-plane modulus and it being difficult to determine the elastic modulus for an out-of-plane angle accurately. The failure for the 45° and 67.5° samples also occurred at a much lower threshold than the other samples due to them having small interlaminar areas between the impact location and edge of the sample and interlaminar shear being the primary means of failure for the 45° and 67.5° samples as seen in Figure 8.

The effect of size of sample was also studied with cubic samples of 35, 50, 65 and 80mm simulated. The damage threshold limit for the 35, 50 and 65mm were similar at approximately 35kN but was higher for the 80mm sample at 45kN. The 35mm sample split during simulation along with the 50mm sample. The 65mm and 80mm samples did not split with the 80mm sample having the most elastic behaviour during unloading. This supports the observation from other tests that interlaminar properties are of utmost importance for in-plane tests. The larger interlaminar area for the larger samples meant that they were more damage resistant in the simulations when comparing sample size. The numerical simulations for 0° samples also provided useful insight into why the samples split off-centre. As seen in Figure 16, lamina buckling occurs directly under the impactor during simulation which leads to the delaminations forming off-centre from the centre of impact by 3-5mm. This lamina buckling causes delaminations to form away from the centre of impact which then propagate into larger delaminations which lead to sample separation at higher loads.

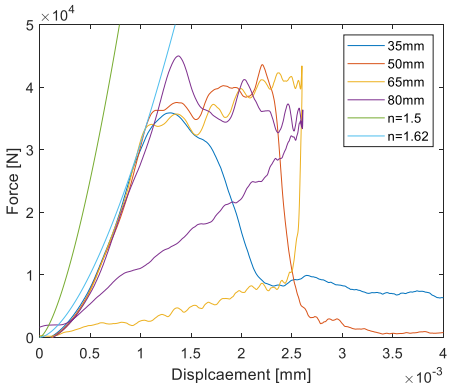

Figure 13. Force-displacement plot for 0° samples at 5m/s

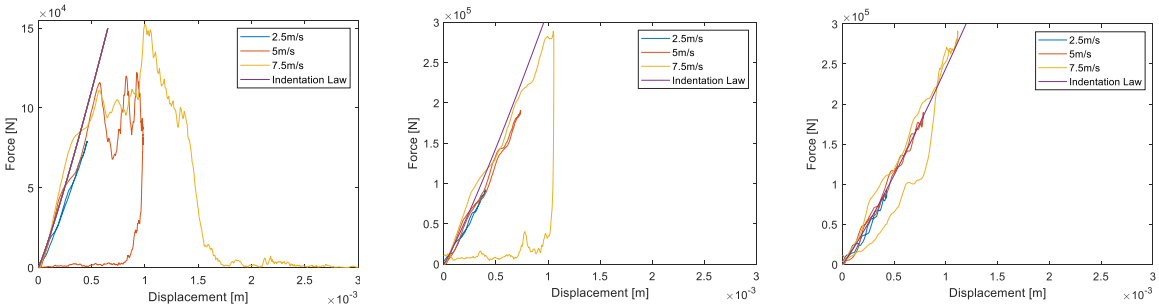

Figure 14. Force-displacement plots for cross-thickness impact of 0° samples at 0° along the plies (left), 45° (centre), and 90° across the plies (right)

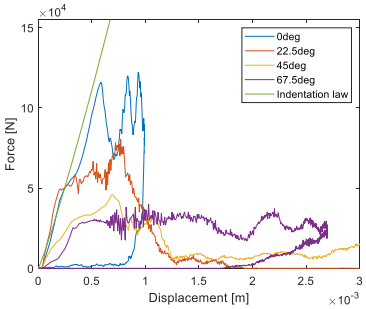

Figure 15. CTI impact on mixed angled samples at 0° along plies (left) and at 90° across plies (right)

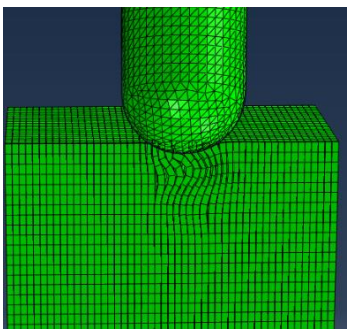

Figure 16 Screenshot of fibre buckling during simulation

V. Summary and Conclusion

The damage progression was clearly identifiable in the experimental testing and can be summarised as follows. Local stress whitening at the contact location of the samples occurred in all tests, however, since the minimum velocity tested was 5m/s further testing at lower velocities would help better identify the threshold at which this starts occurring. This is followed by small delaminations in the local area of impact when the impact force passes the delamination threshold limit. At increasing impact energies, the delamination's propagate until they reach the full depth and width of the sample. When the delaminations have reached the maximum size permitted by sample geometry the interlaminar normal strength is fully compromised and the sample starts to split. The fibres within the lamina can provide a small level of interlaminar strength dependent on the strength of the fibre-matrix interface as discussed and observed from the high-speed footage in Figure . At a certain threshold the contact stresses cause local fibre and matrix crushing in addition to the local stress whitening with severity increasing with impact energy. However, fibre and matrix crushing were only evident in tests at 7.5m/s or higher. The critical damage mechanism for testing was the delamination propagation which led to complete sample failure. While not desirable the stress whitening and fibre and matrix crushing were not critical to the samples damage tolerance when considering sample fracture as the measure for failure.

The analytical model including the Hertzian contact laws modified by Tan and Sun with $n=1.62$ for the hemispherical impactor and Nelson Norden for the cross-thickness impactor represented the nature of the force-displacement relationship well for loading when compared with the experimental and numerical results until the damage threshold limit. Above the damage threshold limit where intense damage occurs including delaminations and fibre-matrix crushing the contact model was no longer accurate. This was expected and in agreeance with other studies published on the topic. For unloading the behaviour was elastic where the damage threshold limit had not been passed and inelastic when it had and the sample did not separate. The Hashin damage criterion modelled the damage of the lamina well in the numerical model however, the critical factor was the interlaminar behaviour not the properties of the lamina.

The numerical model with the mesh used was satisfactory for identifying trends in impact events, however it was shown that a finer mesh could provide much more accurate results. Additional testing for the in-situ material properties of the samples for interlaminar properties may also improve model definition.

Results using the cross-thickness impactor showed that when samples are contacted along the plies in impact there is significantly greater damage with a lower damage threshold limit when compared with contact across plies which resulted in far less damage and a much higher damage threshold limit. The conclusion that interlaminar strength is a key property to be considered during in-plane impact testing was reinforced when the effect of the size of the sample was studied.

In conclusion, this study has examined ultra-thick composite laminates subjected to in-plane impact and will provide a useful basis for further study of the topic of impact on composite marine propellers.

VI. Recommendations

While this study has provided a useful insight for characterising the damage and mechanical behaviour of ultra-thick composites, further study is recommended to bridge the gap between this foundational study using generic samples and impact of a full-scale composite marine propeller in maritime conditions. Better definition of material properties; in particular, testing for interlaminar shear and normal strength is recommended to confirm the accuracy of the numerical model, especially since delaminations were the primary failure mechanism in testing. Use of a version of Abaqus without the restriction of 100,000 nodes will also provide an increase in model accuracy unable to be used in this study. This test has also demonstrated that the interlaminar strength is critical to avert delaminations from forming and propagating. Consequently, investigations for improved through-thickness strengthening is recommended and may include studies into use of a tougher matrix, 3D fibre stitching and use of z-rods.

Acknowledgements

The author would like to thank Prof Evgeny Morozov for his advice and guidance as thesis supervisor. The author would also like to thank Dr Nigel St John and Dr Andrew Phillips of DSTG for their advice, support and Mr Russell Cairns of DST for the manufacture of samples for experimental study. Additionally, the author wishes to thank Prof Paul Hazell for use of the impact dynamics laboratory at UNSW Canberra and Dr Hongxu Wang and other technical staff at UNSW Canberra for their additional support during testing.

References

1. Baley, C., P. Davies, Y. Grohens and G. Dolto, *Application of Interlaminar Tests to Marine Composites. A Literature Review.* Applied Composite Materias, 2004. **11**: p. 99-126.
2. Herath, M.T., *Optimisation of Composite Marine Propeller Blades and Hydrofoils*, in *School of Mechanical and Manufacturing Engineering*. 2016, University of New South Wales Australia. p. 262.
3. Phillips, A.W., M. Pantelidi, J. Salloum, F. Solano and A.C. Orifici. *Low Velocity Impact of Thick Marine Composites*. in *Advancing Composites Innovation Conference*. 2018. Melbourne, Australia.
4. AZOMaterials. *Composite propeller for warship propulsion- construction and advantages of the composite propeller*. 2003 [cited 2018 11 Oct]; Available from: https://www.azom.com/article.aspx?ArticleID=2126.
5. Koko, T.S., K.O.A. Shanin, Unyime O and M.E. Norwood, *Review of composite propeller developments and strategy for modeling composite propellers using PVAST*. 2012, Defence R&D Canada - Atlantic: Halifax.
6. Phillips, A.W., A. Nanayakkara, S. Russo, R. Cairns and N. St John, *Mechanical response of a thick composite hydrofoil*, in *8th Australasian Congress on Applied Mechanics: ACAM 8*. 2014, Engieners Australia: Barton, ACT. p. 673-581.
7. Backman, M.E. and W. Goldsmith, *The mechanics of penetration of projectiles into targets.* International Journal of Engineering Science, 1978. **16**: p. 1-999.
8. Don, K.A. and K. Karunarathna, *Low-velocity impact analysis of monolithic and laminated glass using finite element method (FEM)*, in *School of civil engineering*. 2013, University of Birmingham.
9. Zhang, X., *Predicting low-velocity impact damage in composites by a quasi-static load model with cohesive interface elements.* The Aeronautical Journal, 2012. **116**(1186): p. 1367-1381.
10. Nettles, A. and M. Douglas, *A comparison of quasi-static indentation to low-velocity impact*. 2000, NASA.
11. Reid, S.R. and G. Zhou, *Impact Behaviour of Fibre-Reinforced Composite Materials and Structures*. 2000, Cambridge England: Woodhead Publishing Limited. 303.
12. Highsmith, A.L., *A study of the use of contact loading to simulate low velocity impact.* NASA, 1997.
13. Li, Y., A. Xuefeng and X. Yi, *Comparison with low-velocity impact and quasi-static indentation testing of foam core sandwich composites.* International Journal in Applied Physics and Mathematics, 2012. **2**(1): p. 58-62.
14. Shen, Z., Y.G. Xu and A. Chrysanthou, *Contact Behaviour of Composite Laminate under Quasi-Static Indentation Load.* Key Engineering Materials, 2014. **575-578**: p. 545-548.
15. Guan, Z. and C. Yang, *Low-Velocity Impact and Damage Process of Composite Laminates.* Journal of Composite Materials, 2002. **36**(07): p. 851-871.
16. Xu, Y.G., S. Z, W. Tiu, Y.Z. ZXu, Y. Chen and G. Haritos, *Delamination Threshold Load of Composite Laminates under Low-Velocity Impact.* Key Engineering Materials, 2013. **525-526**: p. 521-524.
17. Zhang, X. and F. Bianacgum, *Predicting low-velocity impact damage in composites by a quasi-static load model with cohesive interface elements.* The Aeronautical Journal, 2012. **116**(1186): p. 1367.
18. Sutherland, L.S. and C.G. Soares, *Contact indentation of marine composites.* Composite Structures, 2005. **70**: p. 287-294.
19. Talagani, M.R., *Impact Analysis of Composite Structures*. 2014, Delft University of Technology.
20. Yang, S.H. and C.T. Sun, *Indentation Law for Composite Laminates*. 1981, Purdue University.
21. Christoforou, A. and A. Yigit, *Transient response of a composite beam subjected to elasto-plastic impact.* Composites Engineering, 1995. **5**(5): p. 459-470.
22. Tan, T. and C.T. Sun, *Use of statical indentation laws in the impact analysis of laminated composite plates.* Journal of Applied Mechanics, 1985. **52**(1): p. 6-12.
23. Nelson Norden, B., *On the compression of a cylinder in contact with a plane surface*. 1973, Institute for basic standards: Washington.
24. Suemase, H., S. Kerth and M. Maeir, *Indentation of spherical head indentors on transversely isotropic composite plates.* Journal of Composite Materials, 1994. **28**(17): p. 1723-1739.
25. Wu, E. and K. Shyu, *Response of composite laminates to contact laods and relationship to low-velocity impact.* Journal of Composite Materials, 1993. **27**(15): p. 1443-1464.
26. Lee, C. and D. Liu, *Effect of impact velocity on the indentation of thick composite laminate.* Society for Experimental Mechanics, 2009(July/August 2009): p. 59-64.
27. Malhotra, A. and F. Guid, *Impact damage to composite laminates: effect of impact location.* Applied Composite Materials, 2014. **21**: p. 165-177.
28. Cai, S., W. Tang and S. Zhang, *Damage behaviour of laminated e-glass/epoxy beams with an initial delamination subjected to an axial impact.* Mechanics of Composite Materials, 2009. **45**(1): p. 33-44.
29. Goldsmith, W., *Impact: the theory and physical behaviour of colliding solids*. 2001, Nineola, NY: Dover Publications.
30. Perillo, G., N.P. Vedvik and A.T. Echtermeyer, *Numerical analyses of low velocity impacts on composite. Advanced modelling techniques.*, in *2012 SIMULIA Communicty Conference*. 2012: Providence RI. p. 1-16.
31. Ravi-Chandar, K., *Impact Response of Helicoidal Composites*. 2011, Center for the Mechanics of Solids, Structures and Materials; The University of Texas at Austin.
32. Chang, F.-K., J.M. Tang and D.G. Peterson, *The Effect of Testing Methods on Shear Strength Distribution on Laminated Composites.* Journal of Reinforced Plastics and Composites, 1987. **6**(4): p. 304-318.
33. Heinz, D., B. Richter and S. Weber, *Application of advanced materials for ship construction - Experiences and problems.* Materials and Corrosion, 2000. **51**: p. 407-412.

34. Kim, J.-K. and M.-L. Sham, *Impact and delamination failure of woven-fabric composites.* Composites Science and Technology, 1999. **60**(5): p. 745-761.
35. Deng, S. and L. Ye, *Influence of Fiber-Matrix Adhesion on Mechanical Properties of Graphite/ Epoxy Composites: I. Tensile, Flexure, and Fatigue Properties.* Journal of Reinforced Plastics and Composites, 1999. **18**(11): p. 1021-1040.
36. Mouritz, A.P., J. Gallagher and A.A. Goodwin, *Flexural Strength and Interlaminar Shear Strength of Stitched GRP Laminates Following Repeated Impacts.* Composites Science and Technology, 1997. **57**: p. 509-522.
37. Mouritz, A.P., K.H. Leong and I. Herszberg, *A review of the effect of stitching on the in-plane mechanical properties of fibre-reinforced polymer composites.* 1997.
38. Rugg, K.L. and B.N.M. Cox, R, *Mixed mode delamination of polymer composite laminates reinforced through the thickness by z-fibers.* Composites Part A: applied science and manufacturing, 2002. **33**: p. 177-190
39. Stig, F., *An Introduction to the Mechanics of 3D-Woven Fibre Reinforced Composites*, in *Aeronautical and Vehicle Engineering*. 2009, Kungliga Tekniska hogskloan: Stockholm. p. 40.
40. Daniel, I., H. Hsiao and S. Wooh, *Failure mechanisms in thick composites under compressive loading.* Composites Part B: Engineering, 1996. **27B**: p. 543-552.
41. Parlevliet, P.P., H.E.N. Bersee and A. Beukers, *Residual stressesin thermoplastic composites - a study of the literature. Part III: Effectsof thermal residual stresses.* Composites Part A: applied science and manufacturing, 2007. **38**: p. 1581-1596.
42. Wang, J., K. Potter, K. Hazra and M. MWisnom, *Experimental fabricatino and characterisation of out-of-plane fiber waviness in continuously fiber -reinforced composites.* Journal of Composite Materials, 2012. **46**: p. 2041-2053.
43. Zhou, G., *Static behaviour and damage of thick composite laminates.* Composite Structures, 1996. **36**: p. 13-22.
44. Hashin, Z., *Failure Criteria for Unidirectional Fiber Composites.* Journal of Applied Mechanics, 1980. **47**(2): p. 329-334.
45. Dassault Systems. *Analysis of composite materials with Abaqus*. 2018 [cited 2018 8 Oct]; Available from: https://www.researchgate.net/profile/Azzam_Ahmed5/post/How_can_I_simulate_progressive_impact_damage_in_composite_material_with_Abaqus/attachment/59d63617c49f478072ea3ef0/AS%3A273658583420928%401442256698532/download/Analysis+of+Composite+Materials+with+Abaqus.pdf.
46. *ABAQUS User's Guide V6.10*. Simulia.
47. Roberts, M.L., *Development of a Finite Element Model for Predicting the Impact Energy Absorbing Performance of a Composite Structure*, in *Mechanical Engineering*. 2014, California Polytechnic State University: California. p. 90.
48. ATLComposites. *Laminating/ R118 Infusion*. 2018 [cited 2018 8 Oct]; Available from: http://atlcomposites.com.au/icart/products/14/images/main/KINETIX%20R118.pdf.
49. Australia, C. *MQ1200D127 - FIBREGLASS STITCHED QUADRAXIAL 0°/90°/+45°/-45° 1205G/M2 1270MM - AUSTRALIAN MADE*. 2018 [cited 2018 08 Oct]; Available from: http://www.colan.com.au/compositereinforcement/stitched/quadraxial/fibreglass-quadraxial-0-90-45-45-1205g-m2-1270mm.html.
50. ATLComposites. *KINETIX R118 infusion system*. 2018 [cited 2018 8 Oct]; Available from: http://atlcomposites.com.au/category/5/Infusion.
51. ATLComposites. *Engineering Data R118 Infusion*. 2018 [cited 2018 8 Oct]; Available from: http://atlcomposites.com.au/icart/products/14/images/main/KINETIX%20R118%20Eng%20Data.pdf.
52. St John, N. and A.W. Phillips, *Expected properties for composite samples*. 2018.
53. Barbero, E., F. Cosso, R. Roman and T. Weadon, *Determination of material parameters for abaqus progressive damage analysis of e-glass epoxy laminates.* Composites: Part B, 2013. **46**: p. 211-220.
54. Nabila, H., S. Hamat, L. Arumugam, A. Umaira, I.M. Alibe, M. Golshan, and D.L. Majid, *Glass/epoxy woven composite laminate design based on nonlnear results.* APRN Journal of Engineering and Applied Sciences, 2015. **10**(21): p. 9992-9998.